Linking Instantaneous and Climatological Perspectives on Eddy-Driven and Subtropical Jets

CLEMENS SPENSBERGER,[a,b] CAMILLE LI,[a,b] AND THOMAS SPENGLER[a,b]

[a] *Geophysical Institute, University of Bergen, Bergen, Norway*
[b] *Bjerknes Centre for Climate Research, Bergen, Norway*

(Manuscript received 9 February 2023, in final form 14 September 2023, accepted 26 September 2023)

ABSTRACT: The distinction between eddy-driven and subtropical jets is conceptually important and well-founded based on different driving mechanisms and dominant types of variability. This climatological perspective may be augmented by considering instantaneous maxima in the wind field and linking these to the time-mean jets. Inspired by EOF and cluster analyses to explore the variability in jet occurrences, we propose a straightforward framework that naturally distinguishes subtropical from eddy-driven jets in instantaneous data. We document that for most ocean basins, there is a clear bimodality in instantaneous jet occurrences in potential temperature–wind speed space. The two types of jets in this phase space align well with the conceptual expectations for subtropical and eddy-driven jets regarding their vertical structure as well as their regional occurrence. Interestingly, the bimodality in phase space is most pronounced in the western North Pacific during winter. The climatological jet in this region is typically regarded as "merged," resulting from a mixture of thermal driving and eddy driving. Our results clarify that the strongest instantaneous jets in this region are classified as subtropical, with eddy-driven jets occurring in close proximity to the climatological mean jet, though weaker and slightly more poleward. We also show that the regions of climatological transition from predominantly subtropical to predominantly eddy-driven jets are just downstream of the strongest climatological jets.

KEYWORDS: Atmospheric circulation; Jets; Storm tracks; Upper troposphere

1. Introduction

The distinction between subtropical and eddy-driven jets is conceptually well-founded (e.g., Lee and Kim 2003; Lachmy and Harnik 2016). Subtropical jets arise due to angular momentum conservation in the upper-tropospheric branch of the Hadley circulation, and thus ultimately due to tropical convection ["thermal driving" in Li and Wettstein (2012)]. In contrast, eddy-driven jets are a result of midlatitude dynamics, specifically the momentum flux convergence associated with midlatitude eddies ["eddy driving" in Li and Wettstein (2012)]. On a month-to-month time scale, these types of jets also exhibit different kinds of variability, with subtropical jets predominantly varying in intensity ("pulsing") and eddy-driven jets predominantly varying in latitude ("shifting") (Eichelberger and Hartmann 2007). It remains unclear, however, to what extent this well-founded distinction carries over to wind maxima on shorter time scales.

Many studies already distinguish between eddy-driven and subtropical jets in instantaneous data (e.g., Koch et al. 2006; Schiemann et al. 2009; Pena-Ortiz et al. 2013; Martius 2014; Manney et al. 2014; Christenson et al. 2017) and thus implicitly assume that the distinction remains valid and sufficiently analogous to the time-mean concept. The separation of the jet types is done using a wide range of criteria and metrics. For example, Koch et al. (2006) devise an index that reflects the differing vertical distribution of wind shear in the troposphere, while Martius (2014) isolate subtropical jets using a combination of criteria based on wind speed on a selected isentropic level and vertical wind shear. Christenson et al. (2017) and Winters et al. (2020a,b) follow a similar approach considering only the isentropic level of the jet core to study jet superposition events. Beyond addressing this specific application, their analysis indicates that potential temperature can more generally be useful as a distinguishing characteristic for instantaneous jet types. Finally, Manney and Hegglin (2018) use the change in Cartesian height of the tropopause across the jet to first identify what are assumed to be instantaneous subtropical jets. They then classify all remaining jet cores poleward of a detected subtropical jet as eddy-driven. Further, if no subtropical jet was found, all jet cores poleward of 40° latitude are taken as eddy-driven. Involving three thresholds and requiring the detection of the tropopause structure, this classification algorithm is rather complex.

On longer time scales, many studies follow Woollings et al. (2010) and consider low-pass-filtered wind in the lower troposphere to isolate eddy-driven jets. For example, the North Atlantic jet regimes introduced by Madonna et al. (2021) are based on this jet definition. The rationale behind this definition is that only eddy-driven jets are expected to have a signature in the lower troposphere in the form of surface westerlies. However, low-level winds are also influenced by other processes, such as the flow distortion around orography (White et al. 2019), complicating the connection between low-level winds and upper-tropospheric dynamics. On such time scales, it would also be possible to base a jet classification directly on indices

Supplemental information related to this paper is available at the Journals Online website: https://doi.org/10.1175/JCLI-D-23-0080.s1.

Corresponding author: Clemens Spensberger, clemens.spensberger@uib.no

DOI: 10.1175/JCLI-D-23-0080.1

TABLE 1. Boundaries for the ocean and continental sectors. The boundaries of the ocean sectors are identical to Spensberger and Spengler (2020).

Sector	Latitude	Longitude	Sector	Latitude	Longitude
North Atlantic	20°–70°N	80°W–10°E	South Atlantic	20°–65°S	65°W–10°E
Asia	20°–70°N	50°–110°E	South Indian Ocean	20°–65°S	25°–115°E
North Pacific	20°–70°N	120°E–120°W	South Pacific	20°–65°S	180°–80°W

capturing the different driving mechanisms [such as in Li and Wettstein (2012)] or predominant modes of variability (Eichelberger and Hartmann 2007), but these approaches are unfortunately not easily extended to instantaneous data. One may speculate, however, that many properties of the climatological distinction between eddy-driven and subtropical jets should emerge naturally from an instantaneous jet classification, as will be shown here.

In addition to the wide variety of approaches for instantaneous and climatological jet classification, some studies suggested that eddy-driven and subtropical jets may be regarded as conceptual extremes of a spectrum of instantaneous jets with varying degrees of midlatitude and tropical origin (Manney et al. 2014; Spensberger and Spengler 2020). Here, we challenge the notion of a spectrum of jets by systematically assessing different approaches to classify instantaneous jets, and documenting two distinct types of jets that link well to the established time-mean concepts (e.g., Lee and Kim 2003; Li and Wettstein 2012). Instead of defining a classification criterion a priori, we systematically explore the patterns of variability of instantaneous jets to identify the criteria that are best able to distinguish between jet types. The criterion that emerges from this procedure is based on potential temperature, as previously suggested by Christenson et al. (2017). This work thus justifies the selection of this criterion, compares its efficacy with respect to other criteria, and systematically explores the links between the emerging instantaneous jet categories and well established concepts of driving mechanisms for time-mean jets.

2. Extracting jet cross sections

We base our analyses on detections of instantaneous jet axes following Spensberger et al. (2017). Jet axes are defined in Spensberger et al. (2017) as lines separating cyclonic from anticyclonic wind shear in the instantaneous two-dimensional flow field on the PV2-surface (i.e., the surface where PV $= 2 \times 10^{-6}$ m^2 s^{-1} K kg^{-1}). They thus trace lines of maximum wind irrespective of the flow direction [illustration of the method in Fig. 1 of Spensberger et al. (2017)]. By using the PV2-surface we detect both subtropical and eddy-driven jets (Spensberger and Spengler 2020). The detection algorithm requires a well-defined wind maximum, which relies on a combination of the sharpness of the wind maximum and the wind speed. For details of the detection algorithm, we refer the reader to Spensberger et al. (2017). For climatologies and a comprehensive overview over the month-to-month variability of the thus-defined jets we refer to Spensberger and Spengler (2020).

We conduct the analyses on 6-hourly data from ERA-Interim (Dee et al. 2011) for the period 1979–2018, and on 3-hourly data from ERA5 (Hersbach et al. 2020) for 1979–2020. An extended set of ERA5 jet detections for 1979–2022 is published in Spensberger (2023a). For both reanalyses, we use data pre-interpolated to pressure levels and the PV2-level as provided by ECMWF. For both reanalyses we use a horizontal resolution of 0.5°. As results are nearly identical between the two reanalyses, we only show results for ERA5. The dataset comprises 3.2×10^6 instantaneous jet axes in ERA5, around 25 per time step. Together, these axes are made up of a total of about 3.8×10^8 point coordinates, each marking the intersection of a jet axis with a grid cell boundary.

To explore the patterns of variability in instantaneous jet structure, we randomly select points from this large database and extract cross sections perpendicular to the jet at these selected points. The grid of the cross sections comprises the cross-jet distance from −500 to +500 km in steps of 50 km (21 grid points in the horizontal, positive on the cyclonically sheared/cold side) and altitude in pressure in steps of 50 hPa. For ERA-Interim we extract data for 950–100 hPa (18 grid points in the vertical). For ERA5 we extend the cross section to 1000–50 hPa and include the 30- and 10-hPa levels in the stratosphere (22 grid points in the vertical). In the horizontal, we use a bilinear interpolation from the model grid to the location of the cross section. For each cross section, we extract temperature, the height of the PV2 surface in pressure, as well as the along-jet and cross-jet components of the wind vector.

For each combination of the four seasons and the five ocean basins (North Atlantic, North Pacific, South Atlantic, south Indian Ocean, and South Pacific) in Spensberger and Spengler (2020) and an additional Asian sector, we extract cross sections for 100 000 randomly selected jet axis points. The latitude and longitude boundaries of these sectors are summarized in Table 1. The resulting dataset of jet cross sections is publicly available (Spensberger 2023b).

In the following, terms such as jet axes, eddy-driven jet and subtropical jet refer to instantaneous jets unless otherwise specified as climatological or time mean.

3. Jets in potential temperature–wind speed space

Inspired by numerous attempts to achieve an automatic jet-type classification through EOF and cluster analyses (cf. section 1 in the online supplemental material), we analyze jet occurrence during winter in the potential temperature–wind speed phase space. Winter is here taken to be DJF in the Northern Hemisphere and JJA in the Southern Hemisphere. Although none of these statistical analyses yielded a satisfactory classification, in synthesis the analyses consistently point to wind speed and jet-core potential temperature as the two dominant dimensions of variability in jet structure. The inclusion of wind

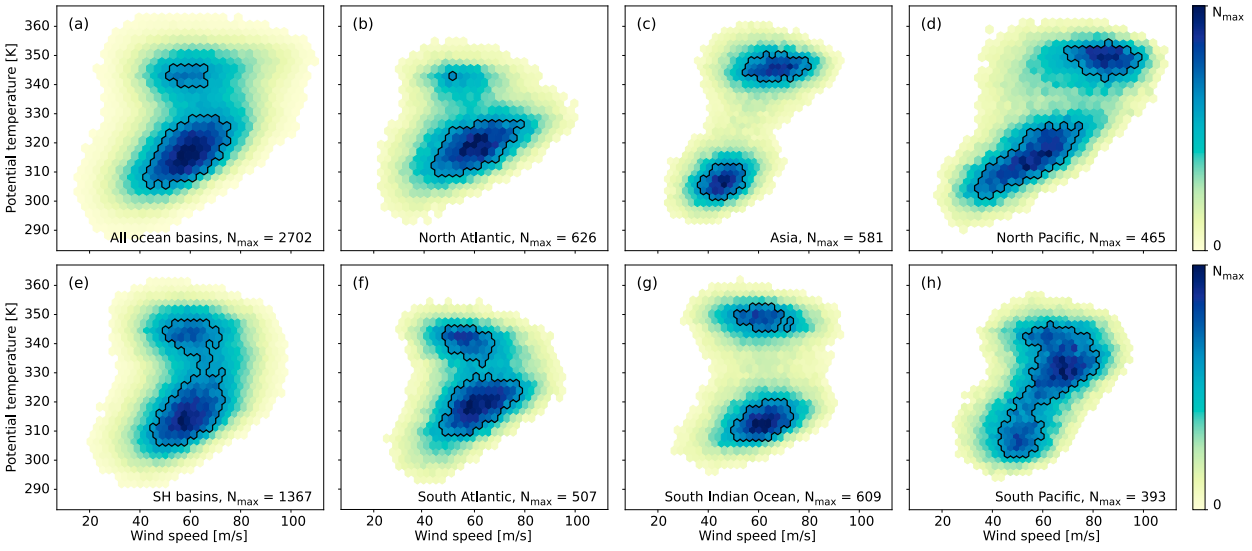

FIG. 1. Two-dimensional histograms of jet occurrence in potential temperature–wind speed space during winter (DJF for Northern Hemisphere and JJA for Southern Hemisphere). (a) Sum of all ocean sectors, (b) North Atlantic, (c) North Pacific, (d) sum of all SH ocean basins, (e) South Atlantic, (f) southern Indian Ocean, and (g) South Pacific. Contours ($0.6N_{max}$) show the most frequently occurring regions in the phase space.

speed as one of the two dimensions is in line with Dorrington and Strommen (2020), who documented that wind speed is an essential parameter to characterize the state of the North Atlantic jet.

The two-dimensional histogram of jet occurrence in potential temperature–wind speed space shows a clear bimodality in most sectors, as well as for the Southern Hemisphere and all storm tracks combined (Fig. 1). One peak in jet occurrence is located between 340 and 350 K and a second, generally wider and deeper peak in occurrence between 310 and 330 K. The degree of separation between these two types of jets varies, being most distinct in the south Indian Ocean (Fig. 1g) and least distinct in the South Pacific (Fig. 1h). Nevertheless, in the South Pacific, a type of jet around 305 K is relatively well separated from one or two types of jets between 325 and 345 K. The latter type shows some internal structure, with slight peaks in the distribution around 330 and 345 K.

Comparing the two ocean basins in the Northern Hemisphere, the histograms might appear counterintuitive. The climatological North Pacific winter jet is often interpreted as "merged," which is driven by both tropical convection and internal midlatitude dynamics (Lee and Kim 2003; Li and Wettstein 2012), yet the separation into two types of instantaneous jets is very clear (Fig. 1d). In contrast, the North Atlantic regularly features geographically well-separated eddy-driven and subtropical jets during the winter season [cf. climatologies in Manney et al. (2014), Spensberger and Spengler (2020)], yet the separation into the two instantaneous jet types in potential temperature–wind speed space is less pronounced than in the North Pacific. We will return to this discussion in more detail in section 3d.

In the above discussion, we have already implicitly associated the two types of jets in the histograms in Fig. 1 with subtropical and eddy-driven jets. Such an association would be a conceptually pleasing match between theory (e.g., Lee and Kim 2003) and observations; it also seems reasonable that subtropical jets occur at higher potential temperature than eddy-driven jets. In fact, the isentropic levels of the two jet types documented here fit well with the height of the Hadley and eddy-driven circulations in Yamada and Pauluis (2015, 2016) and Christenson et al. (2017). To further clarify this correspondence, we assess the different characteristics of the jets in each bin of the histograms (section 3a), compare the two-dimensional structure of the two types of jets (section 3b), and compare their regional occurrence (section 3c).

Here and in the following, we focus on jets during the winter season. Most conclusions remain qualitatively unchanged during summer (cf. Figs. S3–S6 in section 2 of the supplemental material) and the transition seasons [not shown but included in Spensberger (2023b)]. Only the specific isentropic levels vary to some degree across the seasons, as do the relative frequencies of occurrences of high- and low-θ jets, as well as the longitudinal sectors of maximum and minimum separation. Beyond the sectors shown here, the results also carry over to a North American sector (Fig. S7) with jet occurrence similar to the North and South Atlantic (Figs. 1b,f).

a. *Differences in jet characteristics*

The first characteristic that we consider is the (absolute) latitude of the jet core in each bin (Fig. 2). For all ocean basins, the high-θ jets occur at subtropical latitudes between 25° and 35° (Figs. 2a–h). Further, high-θ jets exhibit less variability in latitude than their low-θ counterparts (Figs. 2i–p). Typically, the standard deviation of latitude for high-θ jets is only about 2°–3° latitude. In contrast, low-θ jets generally occur between 40° and 55° off the equator, and are much more variable in

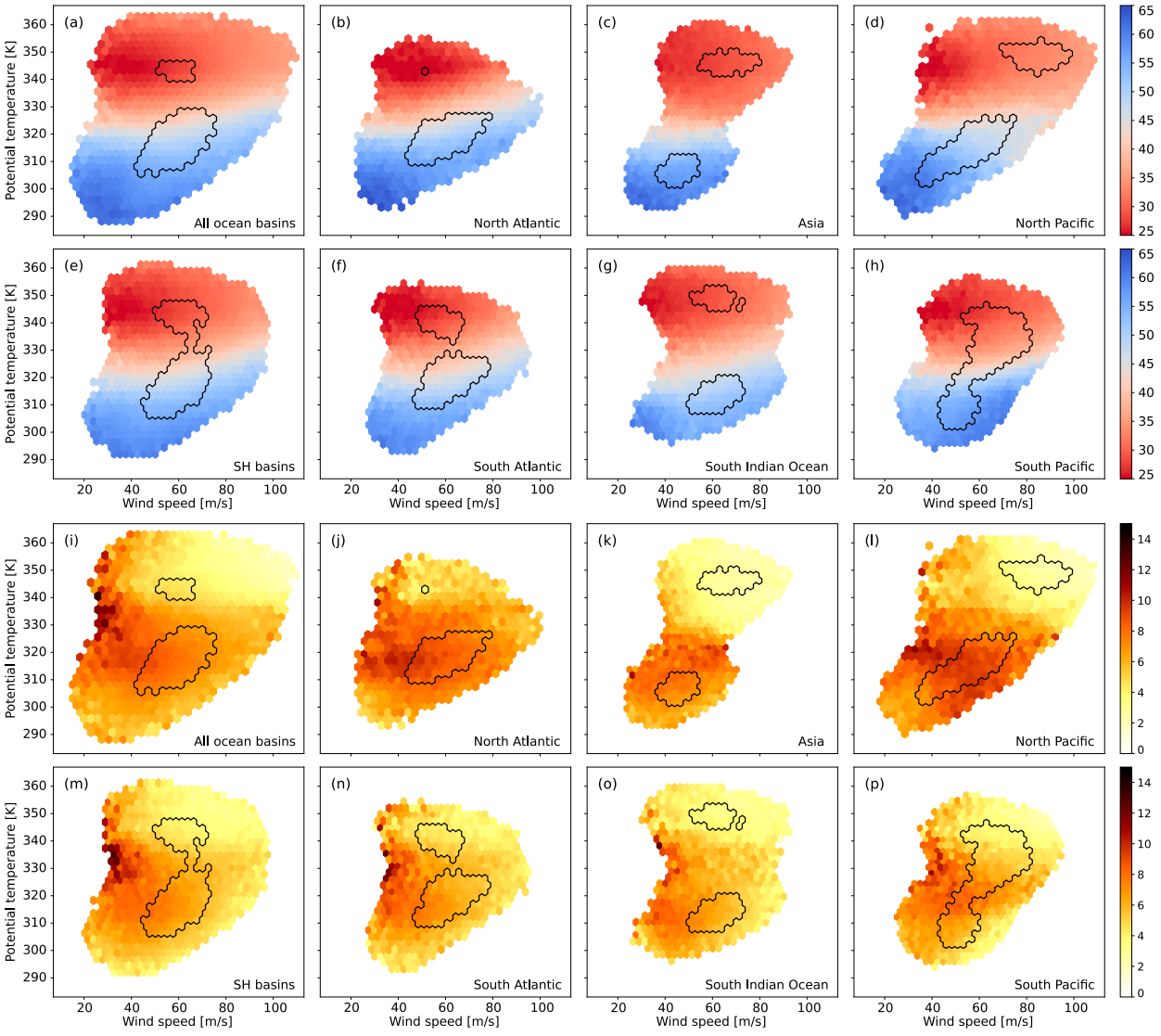

FIG. 2. (a)–(h) Mean and (i)–(p) standard deviation of absolute jet latitude per bin in potential temperature–wind speed space during winter. The panel setup for (a)–(h) and (i)–(p) are as in Fig. 1. Contours show the most frequently realized parts of state space as in Fig. 1.

their latitudinal location with typical standard deviations of 5°–8° latitude.

Both the mean and standard deviation of latitude meet conceptual expectations of subtropical and eddy-driven jets. From both the synoptic and time-mean perspective, the latitude of subtropical jets is set by the poleward extent of the Hadley circulation (Lee and Kim 2003), explaining the more stable position compared to the eddy-driven jet. On monthly and longer time scales, the eddy-driven jet is known to shift latitudinally (Eichelberger and Hartmann 2007), reflecting the varying location of the strongest eddy momentum flux convergence in a given time period. The large variability in latitude of the low-θ jets is consistent with both the varying location of a time-mean jet as well as the variable location of individual eddies. Latitude characteristics thus strongly support the interpretation of our two types of jets as subtropical and eddy-driven.

As several authors identify the eddy-driven jet by considering the low-pass-filtered low-level winds (e.g., Woollings et al. 2010; Madonna et al. 2020), we follow Woollings et al. (2010) and consider the component of 10-day low-pass-filtered wind averaged over 925–700 hPa in the direction of the upper-level jet. Following this definition, the stronger this low-level wind component, the more the jet would be considered eddy-driven. Note that this metric also reflects changes in wind direction between the instantaneous upper-tropospheric winds used for jet detection and the time-filtered low-level winds. We nevertheless use this metric to recreate as closely as possible the diagnostic used in cited studies.

Overall, the relation between the low-level wind and the type of jet is less clear than the relation with latitude (Fig. 3). Nevertheless, high-θ jets are generally associated with weaker or even opposing low-level wind compared to low-θ jets (lighter blues enclosed by the most frequently occurring high-θ jets

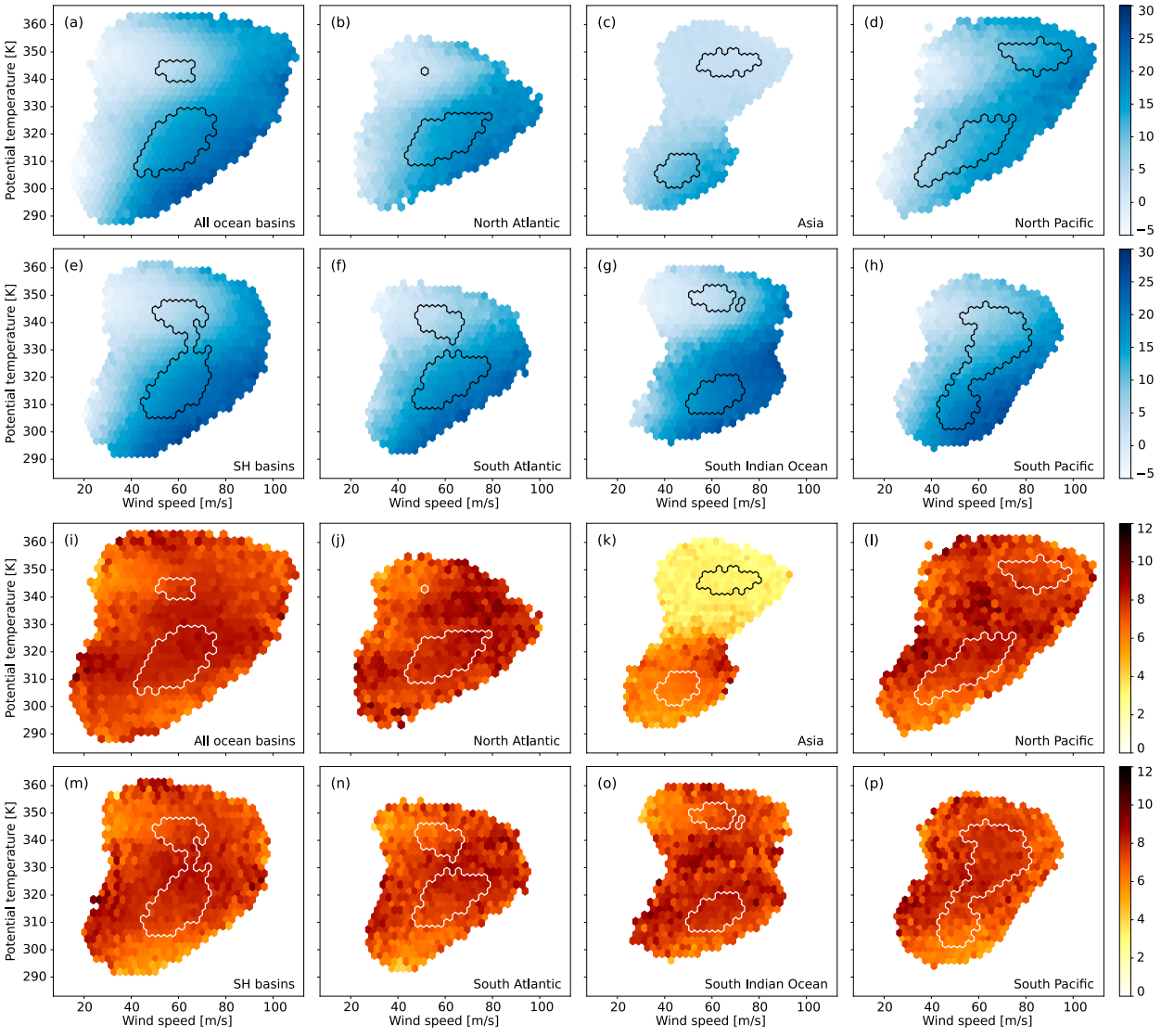

FIG. 3. As in Fig. 2, but for 700–925-hPa wind in the direction of the upper-level jet.

compared those at lower θ in Figs. 3a–h). For low-θ jets, the low-level wind generally follows the jet direction with a wind component of 10–20 m s^{-1}, whereas for high-θ jets this component varies between -5 and $+10$ m s^{-1}.

These two wind speed intervals would be well-separated were it not for the large variability in low-level wind within each bin of the histogram. Throughout the phase space, the variability in low-level wind is around 6–8 m s^{-1} (Figs. 3i–p), comprising a considerable portion of the mean difference between jet types. Thus, while the low-level wind generally supports our interpretation, one has to keep in mind that the relation between our types of jets and low-level wind is much noisier than that for latitude. This is not surprising given that the momentum balance conditions connecting upper- and lower-level winds in the time mean eddy-driven jet do not apply for the instantaneous wind field.

As our third and final jet characteristic, we consider the Koch et al. (2006) wind shear metric Δv_{rel} that was introduced to distinguish between eddy-driven and subtropical jets. The metric is defined as a normalized ratio of wind speed between 200 and 500 hPa:

$$\Delta v_{\mathrm{rel}} = \frac{v_{200} - v_{500}}{v_{200}}, \tag{1}$$

with v denoting the absolute wind speed. As Koch et al. (2006) note, a vertically homogeneous wind shear in isobaric coordinates would yield a value of $\Delta v_{\mathrm{rel}} \approx 0.4$, such that higher values indicate predominantly upper-level baroclinicity and thus a subtropical jet, and lower values indicate predominantly lower-level baroclinicity and thus an eddy-driven jet.

The distribution of mean Δv_{rel} supports previous results (Fig. 4), with the homogeneous-shear line of $\Delta v_{\mathrm{rel}} \approx 0.4$ generally separating the two types of jets (Figs. 4a–h). This separation is, however, clearer in the Atlantic and Indian sectors

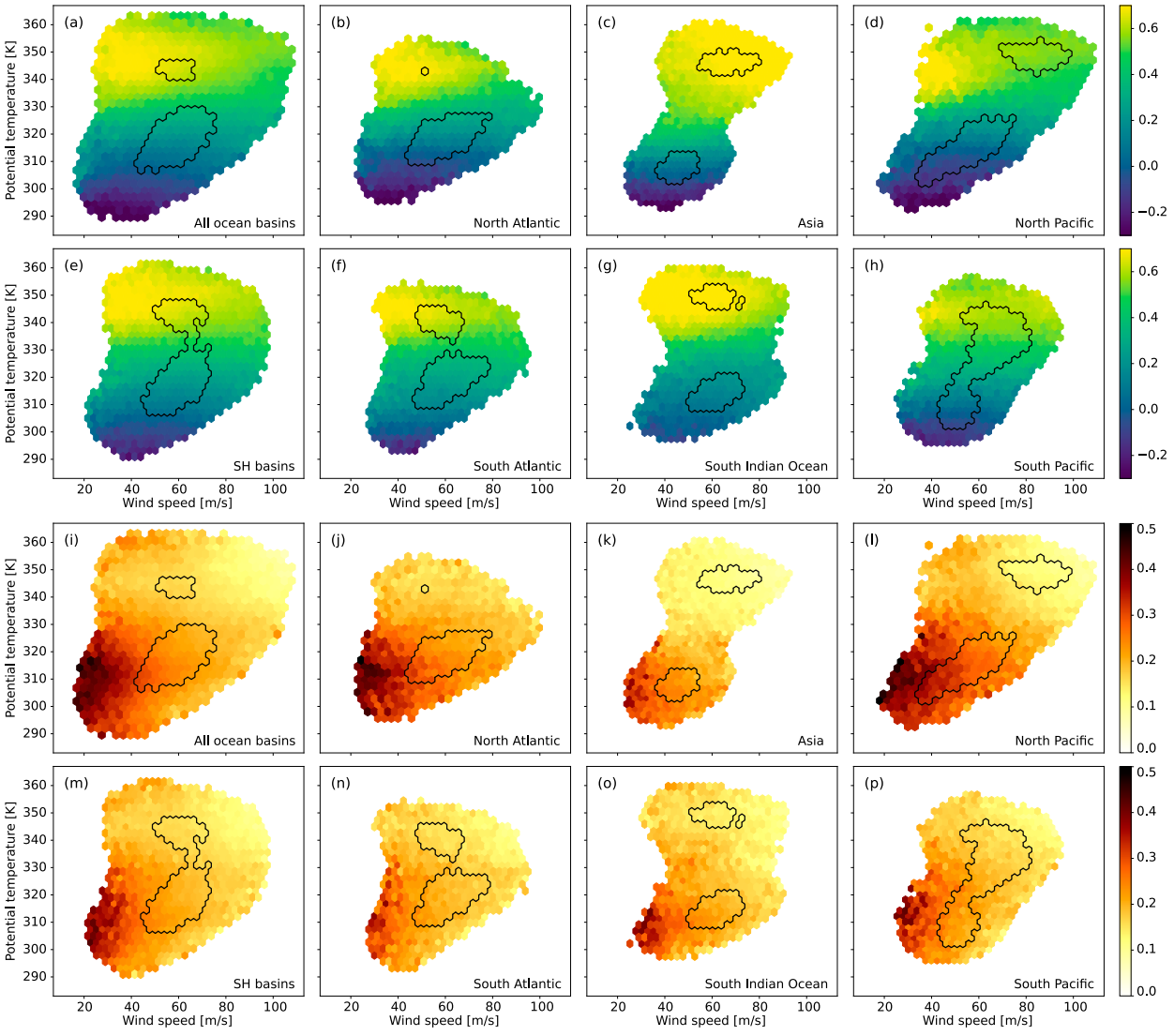

FIG. 4. As in Fig. 2, but for the Koch et al. (2006) metric of vertical wind shear.

compared to the Pacific sectors. In both the North and South Pacific, Δv_{rel} only slightly exceeds 0.4 even for the highest of the commonly occurring jets (within the black contour; Figs. 4d,h). Nevertheless, high-θ jets exhibit distinctly higher values of the shear metric than lower-θ jets even in these ocean basins. In all ocean basins, the lowest of the commonly occurring jets approach $\Delta v_{\mathrm{rel}} = 0$ (Figs. 4a–h), indicating that nearly all of the remaining baroclinicity is in the lower troposphere.

Analogously to latitude, high-θ jets systematically exhibit less variability in Δv_{rel} compared to low-θ jets. Thus, high-θ jets are not just comparatively uniform in meridional occurrence, but also in their vertical structure. The lowest variability among high-θ jets occurs in the Northern Hemisphere in the Asian and Pacific sectors. For these jets, Δv_{rel} is only slightly larger than 0.4, indicating a consistently nearly homogeneous distribution of baroclinicity throughout the troposphere. In other sectors, the standard deviation of Δv_{rel} for high-θ jets is slightly larger with typical values of 0.15–0.2. This variability must, however, still be considered moderate compared to the typical difference between low- and high-θ jets, which is on the order of 0.4–0.5 for all sectors.

In summary, all three jet characteristics considered support the interpretation of the high- and low-θ instantaneous jets as subtropical and eddy-driven, respectively. We document a clear and consistent relation between jet type and both jet latitude and the Koch et al. (2006) shear metric. For low-pass-filtered low-level wind speed, the relation to jet type is not inconsistent with our interpretation, but turns out to be noisier than for the other metrics.

b. *Differences in the two-dimensional structure*

To further corroborate our findings, we consider the two-dimensional structure of the jet in vertical cross sections across the jet core. To this end, we subdivide the potential

temperature–wind speed phase space into four bins for which we construct composites. We first separate low-θ from high-θ jets using a threshold of 335 K, and then further subdivide each type of jet into a weak and strong category based on the respective median wind speed for the ocean sector and altitude category. Thereby, all jet events in the repository of jet cross sections are represented by one of the four resulting categories—in contrast to typical definitions of index-based composites where often events within ± 0.5 or ± 1 standard deviation are not included in any composite. While none of the ocean sectors exhibits a bimodality in jet strength, the subdivision by wind speed nevertheless aids the interpretation of the composites.

The composite structure of the jets is generally consistent across the different ocean sectors (i.e., each column of Fig. 5). high-θ jets generally have shallower jet cores concentrated in the upper troposphere with a maximum wind speed around 200 hPa or 350 K, while low-θ jets have a deeper structure extending down into the midtroposphere with a maximum wind speed around 250 hPa or 325 K. In all ocean sectors, weak high-θ jets are particularly shallow and extend further equatorward than weak low-θ jets (leftmost column in Fig. 5).

High- and low-θ jets also differ clearly in their baroclinic structure (Fig. 5). For high-θ jets, the isentropes in the mid and lower troposphere are only slightly tilted and most of the baroclinicity is located above about 400 hPa (leftmost columns in Fig. 5). Progressing through the columns of Fig. 5 from the left to the right, the baroclinicity first extends downward into the mid and lower troposphere, then decreases from strong to weak low-θ jets.

The category of strong low-θ jets is thus associated with the largest baroclinicity in the lower troposphere and the strongest low-level winds (middle-right column in Fig. 5). The composite maximum wind as well as the vertical and horizontal extent vary only slightly between sectors. Weak low-θ jets vary somewhat more in strength across sectors, but are structurally very similar to their stronger counterparts. If anything, weaker low-θ jets are somewhat more confined in the cross-jet direction.

The arrangement of the columns in Fig. 5 reflects what we see as a natural ordering of these four jet categories. The progression across columns shows gradual changes that are readily and physically interpretable: moving from left to right, the jets shift down in altitude and become deeper in structure. This property would be lost for any permutation of the columns (beyond a trivial reversal). Analogous orderings also exist for nearly all jet categories derived from cluster analyses based on different variables and numbers of clusters (illustration for five clusters in the North and South Atlantic in Fig. S2), suggesting that the ordering reflects a progression along a natural continuum.

The observed differences in structure are also consistent with differences in the driving mechanisms for subtropical and eddy-driven jets. Subtropical jets gain momentum through angular momentum conservation associated with the poleward flow in the upper branch of the Hadley cell (Held and Hou 1980). This is consistent with a shallower jet structure evident in particular on the equatorward side of the high-θ jets (the equatorward/warm side is denoted by negative cross-jet distance in Fig. 5). Eddy-driven jets arise from the action of midlatitude eddies converging zonal momentum in the upper troposphere, The momentum is then transferred to the surface through form drag (e.g., Vallis 2006), such that we would expect a deep structure, consistent with the structure of instantaneous low-θ jets in Fig. 5.

Note that the observed instantaneous jets in Fig. 5 do not differ strongly in width. If anything, instantaneous eddy-driven jets appear to be somewhat narrower than instantaneous subtropical jets. This observation contrasts with the structure of time-mean jets, where eddy-driven jets are clearly broader than time-mean subtropical jets. While instantaneous eddy-driven jets might be somewhat narrower, they occur over a wide range of latitudes due to the fact that eddy driving acts to produce shifting variability in the jet position (consistent with out Figs. 2i–p). For instantaneous subtropical jets, the argument is vice versa; here the small variability in preferred location yields a narrow time-mean jet.

c. *Differences in geographical occurrence*

As a third and final approach to evaluate our jet classification, we consider the regional occurrence of high- and low-θ jets (Fig. 6). Note that the analyses in this section are based on the complete database of jet axis lines (including on the order of 10^7 point coordinates per sector and season), not only the 10^5 points selected for the cross sections.

In both hemispheres, high-θ jets generally occur in narrow annular bands at subtropical latitudes (Figs. 6a,c). Only the Northern Hemisphere features hints of a spiraliform structure in the climatology, with high-θ jets at very low latitudes over the eastern Atlantic and the African continent, then crossing the 30°N line poleward over Asia (Fig. 6a).

In the climatologies, there is little spatial overlap in the occurrence of high- and low-θ jets (cf. Fig. 6a and Fig. 6b; Fig. 6c and Fig. 6d). Only the Northern Hemisphere features a narrow transition zone close to the climatological maximum wind in the western North Pacific and the eastern United States, where high- and low-θ jets each occur for at least in 1%–2% of the time steps. However, nearly all Southern Hemisphere low-θ jets, and most of those in the Northern Hemisphere, occur clearly poleward of high-θ jets. In both hemispheres, low-θ jets occur frequently poleward of 60°–65°. All of these results agree well with the separate climatologies of subtropical and polar jet frequency distributions in the supplemental material of Manney and Hegglin (2018, their Figs. S1, S2, S5, and S6).

The mean potential temperatures at the jet core within each regional bin are consistent with the regional distribution of low- and high-θ jets (Figs. 7a,e). The variability in potential temperature across different jet events in the same geographical bin is largest in those regions where both eddy-driven and subtropical jets can occur. These regions tend to sit poleward of zones with the climatologically strongest wind, more or less collocated with the strongest climatological potential temperature gradient (cf. Figs. 7a,e and Figs. 7b,f). In the Northern Hemisphere, the largest variability in jet-core potential temperature is over the Asia–Pacific sector, while in the Southern Hemisphere it is located in the Indian Ocean–Australian sector (Figs. 7b,f).

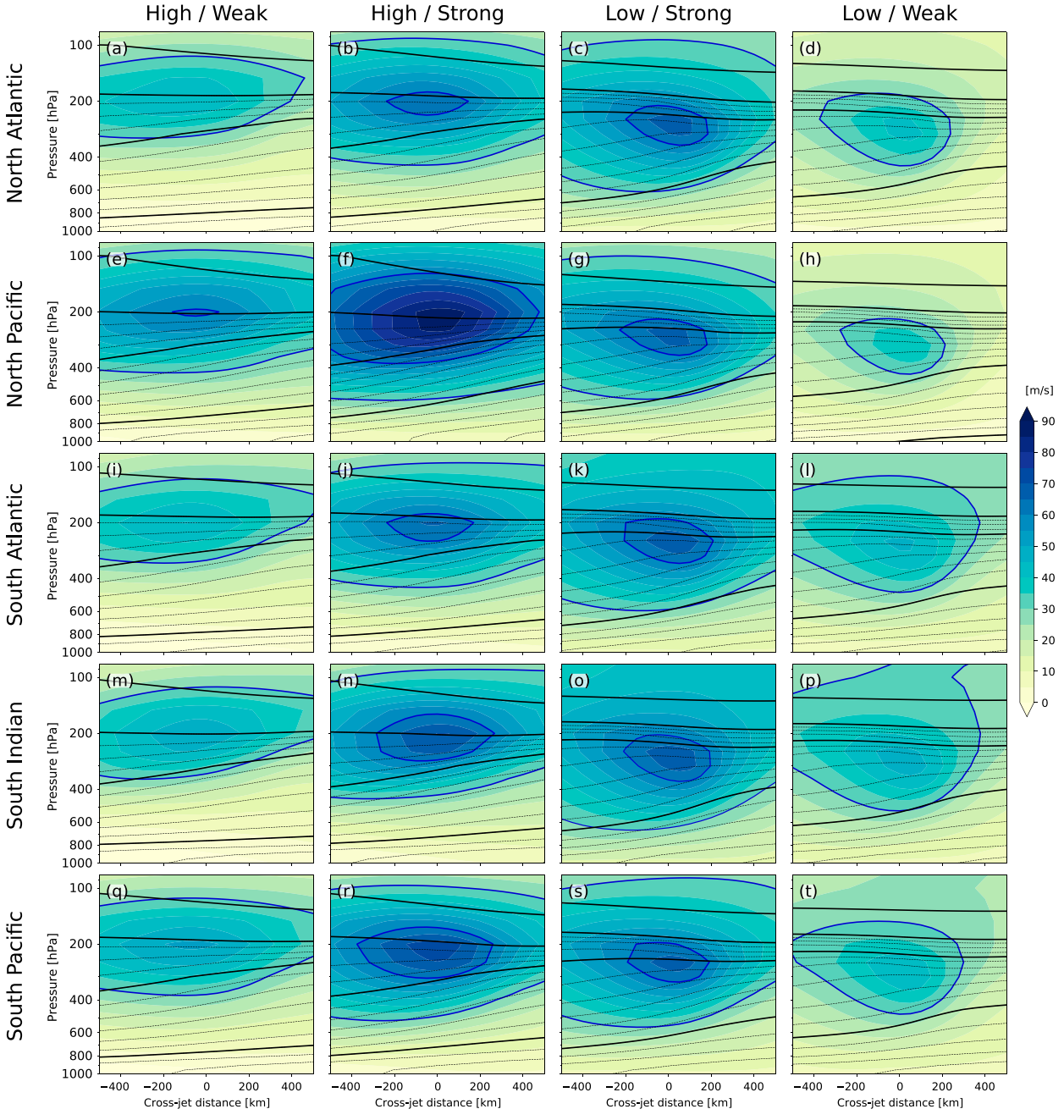

FIG. 5. Composite jet cross sections for high- and low-θ as well as weak and strong jets. The shading shows wind speed and black contours indicate potential temperature with a contour interval of 5 K up to 350 K. The 270-, 300-, 330-, 350-, and 385-K contours are highlighted. Dark blue contours highlight the 30 and 60 m s^{-1} isotachs.

The strongest jets occur on the upstream sides of the Northern Hemisphere ocean basins (Fig. 7c). In both the North Atlantic and North Pacific, the average wind speed at the jet core exceeds 65 m s^{-1}. Remarkably, in terms of average wind speed at the jet core, North Atlantic jets are nearly as strong as North Pacific jets, whereas the climatological mean wind is about 20 m s^{-1} higher in the North Pacific. This indicates that the weaker mean wind in the North Atlantic is mostly due to a more variable jet position rather than a weaker jet and storm track. Manney et al. (2014) published a similar analysis in their Fig. 2e, but document a 5–10 m s^{-1} difference in jet-core wind speed between the North Atlantic and the North Pacific. This might be due to either the use of a different dataset (MERRA versus ERA5), or due to differences in the detection algorithm.

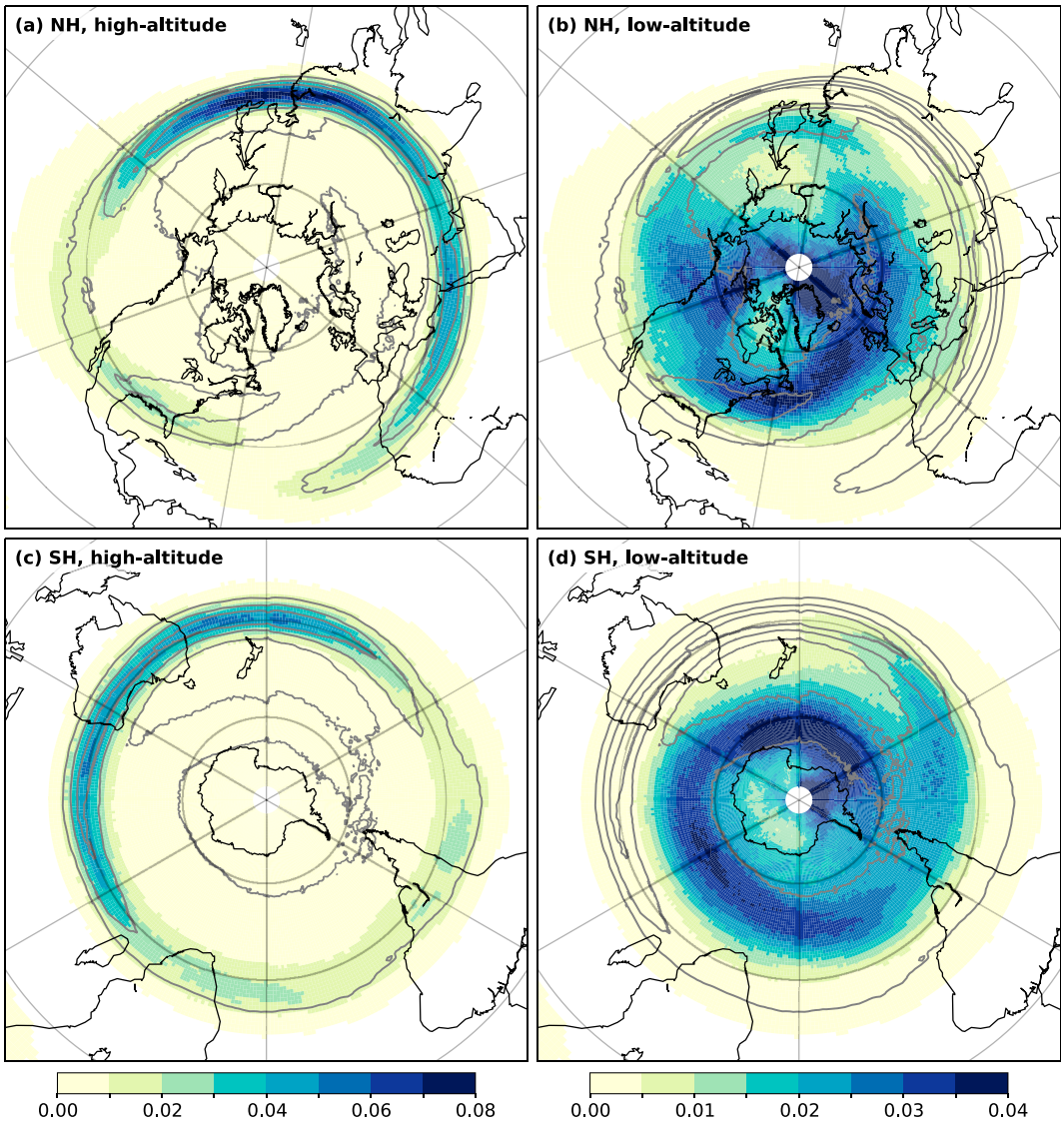

FIG. 6. Frequency of occurrence in 1° × 1° bins of (a),(c) high-θ and (b),(d) low-θ jets in (a),(b) the Northern Hemisphere and (c),(d) the Southern Hemisphere. Gray contours show winter mean wind speed on the PV2 level with a contour interval of 30 m s^{-1}. The figure is based on all jets in the archive rather than the set of cross sections.

In the Southern Hemisphere, the mean wind speed at the jet core is more zonally symmetric than in the Northern Hemisphere (Fig. 7g). The mean jet-core wind varies only between 55 and 65 m s^{-1} throughout large parts of the southern midlatitudes. The most pronounced inhomogeneity in jet-core speed is in the western South Pacific, where both the climatologically strongest and weakest jets of the Southern Hemisphere occur at subtropical latitudes and around 45°S, respectively.

In both Hemispheres, the jet-core speed varies the most on the poleward and downstream side of the climatologically strongest jets (Figs. 7d,h). In the Northern Hemisphere, these regions are located in the northwestern Atlantic and Pacific, respectively. In the Southern Hemisphere they are located poleward of the strong subtropical jet in the Australian sector and western Pacific as well as the central South Atlantic. Given the location poleward and downstream of the strongest jets, we speculate that these regions might be intermittently influenced by the poleward and downstream propagation of intense baroclinic eddies [consistent with the largest storm-track eddy covariances in Chang et al. (2002) and Li and Battisti (2008)].

d. What about merged jets?

We have now comprehensively characterized the properties of low- and high-θ jets. We considered jet latitude, low-level wind, and vertical shear (section 3a, Figs. 2–4), the full jet structure (section 3b, Fig. 5), and their regional occurrence (section 3c, Figs. 6 and 7). All of these analyses support the interpretation of instantaneous low- and high-θ jets as eddy-driven and subtropical jets, respectively. We thus conclude, in

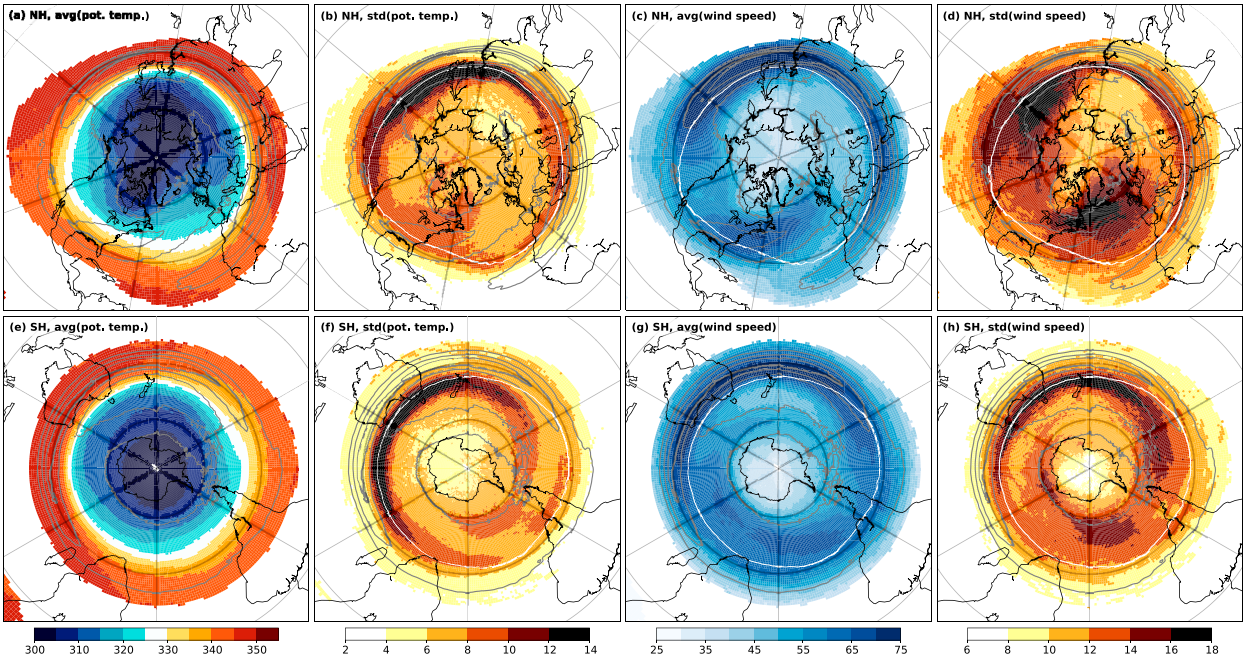

FIG. 7. Mean and standard deviation of jet properties at the level of the maximum wind in 1° × 1° bins. (a),(b),(e),(f) Potential temperature (K) and (c),(d),(g),(h) wind speed (m s^{-1}) at the jet core. (a)–(d) NH and (e)–(h) SH. Gray contours show winter mean wind speed on the PV2 level with a contour interval of 30 m s^{-1}. The white contour in (b)–(d) and (f)–(h) shows the 335 K based on the field in (a) and (e). The figure is based on all jets in the archive rather than the set of cross sections.

line with Christenson et al. (2017), that one can distinguish between instantaneous subtropical and eddy-driven jets using a potential temperature threshold of about 335 K.

This conclusion sheds new light on the prevailing interpretation of the climatological North Pacific jet as "merged" (e.g., Lee and Kim 2003; Li and Wettstein 2012), i.e., a mixture of subtropical and eddy-driven jets. In the phase space histogram for the North Pacific (Fig. 1d), however, the bimodality between the two jet types is pronounced with the vast majority of the strongest instantaneous jets belonging to the subtropical category (Fig. 1d), collocated with the climatological jet (Fig. 6a). Instantaneous eddy-driven jets are much weaker (Fig. 1d) and occur in close proximity though slightly poleward of the climatological jet (Fig. 6b). It is thus predominantly instantaneous subtropical jets that determine the strength and position of the climatological Pacific jet, with instantaneous eddy-driven jets contributing an eddy-driven signature on the poleward flank. Compared to instantaneous subtropical jets in other sectors, the North Pacific ones are more poleward in latitude (Fig. 2d), have stronger lower-tropospheric winds (Fig. 3d) and exhibit less vertical shear (Fig. 4d), all of which are consistent with a merged signature in the climatology.

Besides this issue of classification for the North Pacific winter jet, the clear bimodality raises a more fundamental conceptual issue. Both Manney et al. (2014) and Spensberger and Spengler (2020) document the occurrence of jets following a storm track that gradually spirals poleward in both hemispheres. This result strongly suggests a gradual transformation of jets from purely subtropical to more and more eddy-driven along the spiral. Such a gradual transition appears incompatible with our either–or categorization of jets.

A potential way to reunite the two perspectives might be through the gradual changes in jet vertical structure across the columns in Fig. 5, in which baroclinicity first increases and extends further into the troposphere before it decreases in the transition from strong to weak eddy-driven jets. The suggested progression from weaker subtropical jets via stronger subtropical and stronger eddy-driven jets to weaker eddy-driven jets would be well in line with the continuous spiral structure across latitudes in Manney et al. (2014) and Spensberger and Spengler (2020) as well as the jet properties in Figs. 6 and 7. In the North Atlantic, North Pacific, and South Pacific, the transition from predominantly subtropical to predominantly eddy-driven jets across the ocean basins occurs just downstream of the region with the climatologically strongest jets.

4. Alternative distinctions between eddy-driven and subtropical jets

In previous sections, we have shown that low- and high-θ jets map well onto eddy-driven and subtropical jets, respectively, based on considerations in wind speed–potential temperature phase space. But is this phase space the most suitable to base our analysis on? And how sensitive are our conclusions to this choice? To address these questions, we compare alternative jet phase spaces including latitude (inspired by, e.g., Pena-Ortiz et al. 2013; Manney et al. 2014, and acknowledging that both papers point out severe limitations of this approach), low-level

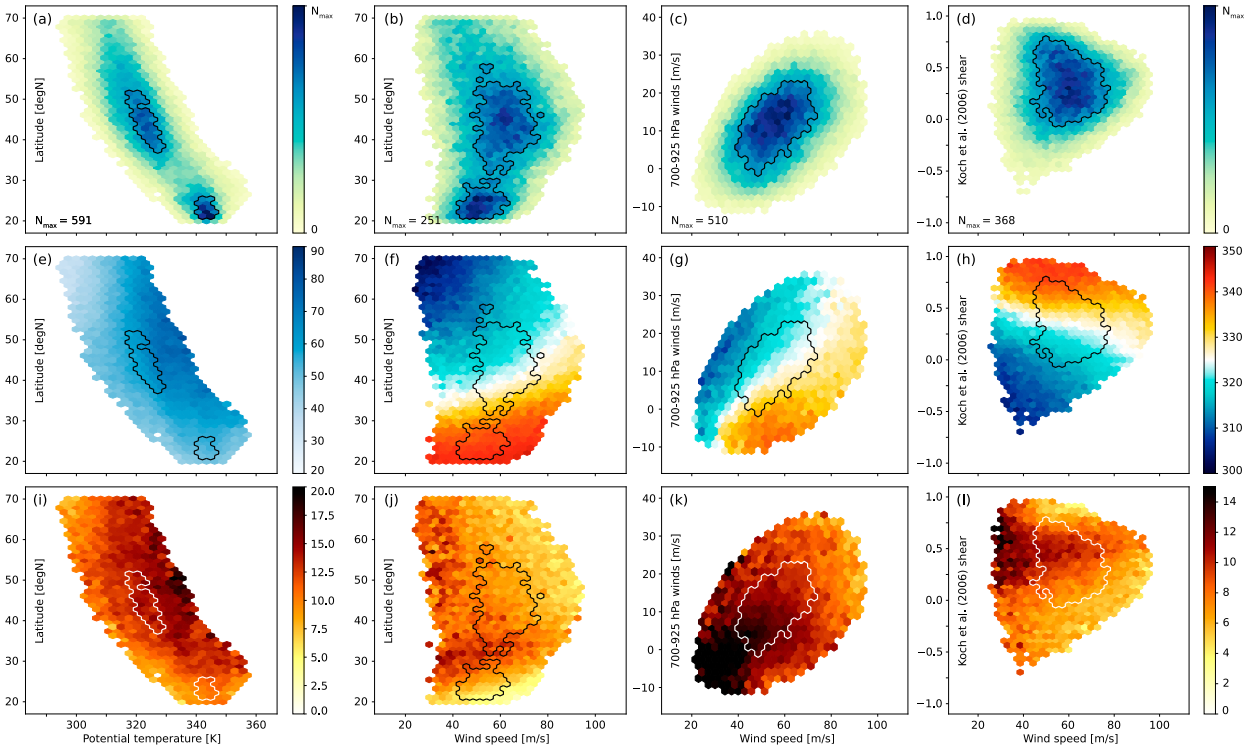

FIG. 8. Alternative phase spaces for North Atlantic jets. Each column shows a different phase space. (from left to right) Based on potential temperature and latitude, wind speed and latitude, wind speed and low-level winds, and wind speed and the Koch-shear metric, respectively. (a)–(d) Two-dimensional histograms analogous to Fig. 1. (e)–(h) Mean and (i)–(l) standard deviation of (a),(e),(i) potential temperature and (b)–(d), (f)–(h),(j)–(l) wind speed.

winds (following, e.g., Woollings et al. 2010), or vertical wind shear (following Koch et al. 2006) as a phase space coordinate instead of wind speed or potential temperature. We then repeat some of our previous analyses based on these alternative phase spaces (Fig. 8). For the sake of brevity we focus this discussion on the North Atlantic and only note differences between sectors where particularly pronounced.

Replacing either potential temperature or wind speed by latitude also yields a bimodal jet distribution in phase space (Figs. 8a,b). Latitude is strongly correlated with jet-core potential temperature (Fig. 8a), thus the 2D histogram retains some of the bimodality that is evident for potential temperature. However, due to the strong correlation between potential temperature and latitude, information about the jet-core speed is largely lost if these two variables are used to define the phase space (Figs. 8e,i), leading to only weak variations in mean speed across this phase space (Fig. 8e) and a large variability within each bin (Fig. 8i).

The bimodality is less pronounced when using latitude *instead of* potential temperature (Fig. 8b). Nevertheless, potential temperature varies clearly across the latitude–wind speed phase space (Fig. 8f), while showing only moderate variability within most bins (Fig. 8j). Latitude can thus to some extent replace potential temperature in our classification. Note, however, that latitude is less bimodal in the North Pacific, where the latitude distribution has one peak at subtropical latitudes and a long tail into mid- and high latitudes [not shown, but in line with findings for this and other sectors in Schiemann et al. (2009), Pena-Ortiz et al. (2013), and Manney et al. (2014)]. A classification based on latitude will thus be somewhat less consistent across sectors.

Using either low-level wind or the Koch et al. (2006) vertical wind shear metric instead of potential temperature, the bimodality vanishes entirely (Figs. 8c,d). For low-level wind, the relation to jet type becomes nontrivial, because for every low-level wind speed one can find both low- and high-θ jets as well as weak and strong jets (Fig. 8g). Further, the mean potential temperature differences across the phase space are less pronounced compared to the latitude and wind shear-based phase spaces (cf. Fig. 8g with Figs. 8f,h), consistent with large potential temperature variability within each bin (Fig. 8k).

Finally, the Koch et al. (2006) wind shear shows a clear relation to potential temperature (Fig. 8h), but also features large variability in potential temperature for values between $\Delta v_{\mathrm{rel}} = 0.3$ and 0.6 (Fig. 8l), which is around the value of $\Delta v_{\mathrm{rel}} \approx 0.4$ that Koch et al. (2006) suggest as a threshold between subtropical and eddy-driven jets. For values outside this range, Figs. 8h and 8l show a clear relation between potential temperature and wind shear with only moderate variability. For unequivocal cases of subtropical and eddy-driven jets, potential temperature and the shear metric thus agree in their classification.

In summary, potential temperature is unique among the analyzed jet characteristics in that it features a pronounced bimodal

distribution in nearly all sectors. This property makes potential temperature particularly well-suited for a jet-type classification. If jet-core potential temperature is not available, it can to some extent be replaced by jet latitude. In contrast, using wind shear or low-level wind, the bimodality is lost. Finally, the relation between low-level wind and the jet is very noisy, such that low-level wind is not suitable for classifying instantaneous jets as subtropical or eddy-driven.

5. Discussion and conclusions

We have documented a clear distinction between two types of instantaneous jets, which, in most sectors and seasons, are clearly separated from each other by jet-core potential temperature. This bimodality in jet-core potential temperature has previously been noted by Christenson et al. (2017). We find these two types of instantaneous jets to align well with the conceptual expectations for eddy-driven and subtropical jets, respectively. We thus conclude that the instantaneous jet-type classification based on potential temperature is well-suited to extend these time-mean concepts to synoptic meteorology and instantaneous jets. We hope that this linkage will provide the foundation for further work bridging the gap between the time-mean and synoptic perspectives on storm-track dynamics.

A further step in this direction would be to extend our analysis to increasingly time-filtered jets. This would allow to thoroughly establish whether the assumptions of Woollings et al. (2010), Madonna et al. (2021) and other studies using low-level winds as a proxy for the eddy-driven jets are permissible in that the relation between jet type and low-level winds becomes more robust through time-averaging. Based on Dorrington and Strommen (2020), we would expect that the jet-core speed remains one of the dominant dimensions of variability between jet events, such that the potential temperature–wind speed phase space used here might remain a useful tool also for time-filtered jets.

Based on our instantaneous classification, the climatological "merged" jet in the North Pacific mainly comprises strong subtropical jets, with weaker eddy-driven jets occurring on the poleward flank of the climatological mean jet. Hence, while the strength and position of the climatological mean jet in the North Pacific is dominated by instantaneous subtropical jets, the weaker instantaneous eddy-driven jets in close proximity yield the eddy-driven signature previously identified in the literature.

We further show that among the considered characteristics, potential temperature is the variable that is best suited to discriminate between the two jet types. Potential temperature is highly correlated with jet latitude, such that latitude can to some extent be used to substitute potential temperature. The distribution of latitude is, however, less bimodal than that of potential temperature. A threshold latitude would thus be a more subjective choice than a threshold potential temperature.

The documented bimodality in jet types might seem at odds with the notion of a spectrum of jet types between purely eddy-driven and purely subtropical [as suggested by Manney et al. (2014) and Spensberger and Spengler (2020)]. In the bimodal distribution, the vast majority of jet events belong to one clearly defined category and are not a blend between them. A spectrum of jet types might still be recovered by considering the gradual changes in jet structure across different jet altitude and strength categories. Both similarity in structure as well as regional occurrence suggest that the transitions from the subtropical to the eddy-driven category predominantly occur for the strongest jets. Further analyses will show to what extent the same idea allows us to reconcile bimodal jet types with the gradual poleward spiraling jet climatologies in Manney et al. (2014) and Spensberger and Spengler (2020).

Acknowledgments. We thank Romain Nurel for carrying out some of the initial exploratory analyses. We thank Gloria Manney and two anonymous reviewers for comprehensive and constructive feedback that helped to considerably improve the manuscript. We acknowledge support from the Nansen Legacy project funded by the Research Council of Norway (Grant 276730).

Data availability statement. The jet detections and cross sections used in this study are published in Spensberger (2023a,b).

REFERENCES

Chang, E. K. M., S. Lee, and K. L. Swanson, 2002: Storm track dynamics. *J. Climate*, **15**, 2163–2183, https://doi.org/10.1175/1520-0442(2002)015<02163:STD>2.0.CO;2.

Christenson, C. E., J. E. Martin, and Z. J. Handlos, 2017: A synoptic climatology of Northern Hemisphere, cold season polar, and subtropical jet superposition events. *J. Climate*, **30**, 7231–7246, https://doi.org/10.1175/JCLI-D-16-0565.1.

Dee, D. P., and Coauthors, 2011: The ERA-interim reanalysis: Configuration and performance of the data assimilation system. *Quart. J. Roy. Meteor. Soc.*, **137**, 553–597, https://doi.org/10.1002/qj.828.

Dorrington, J., and K. J. Strommen, 2020: Jet speed variability obscures Euro-Atlantic regime structure. *Geophys. Res. Lett.*, **47**, e2020GL087907, https://doi.org/10.1029/2020GL087907.

Eichelberger, S. J., and D. L. Hartmann, 2007: Zonal jet structure and the leading mode of variability. *J. Climate*, **20**, 5149–5163, https://doi.org/10.1175/JCLI4279.1.

Held, I. M., and A. Y. Hou, 1980: Nonlinear axially symmetric circulations in a nearly inviscid atmosphere. *J. Atmos. Sci.*, **37**, 515–533, https://doi.org/10.1175/1520-0469(1980)037<0515:NASCIA>2.0.CO;2.

Hersbach, H., and Coauthors, 2020: The ERA5 global reanalysis. *Quart. J. Roy. Meteor. Soc.*, **146**, 1999–2049, https://doi.org/10.1002/qj.3803.

Koch, P., H. Wernli, and H. C. Davies, 2006: An event-based jet-stream climatology and typology. *Int. J. Climatol.*, **26**, 283–301, https://doi.org/10.1002/joc.1255.

Lachmy, O., and N. Harnik, 2016: Wave and jet maintenance in different flow regimes. *J. Atmos. Sci.*, **73**, 2465–2484, https://doi.org/10.1175/JAS-D-15-0321.1.

Lee, S., and H.-K. Kim, 2003: The dynamical relationship between subtropical and eddy-driven jets. *J. Atmos. Sci.*, **60**, 1490–1503, https://doi.org/10.1175/1520-0469(2003)060<1490:TDRBSA>2.0.CO;2.

Li, C., and D. S. Battisti, 2008: Reduced Atlantic storminess during Last Glacial Maximum: Evidence from a coupled climate

model. *J. Climate*, **21**, 3561–3579, https://doi.org/10.1175/2007JCLI2166.1.

——, and J. J. Wettstein, 2012: Thermally driven and eddy-driven jet variability in reanalysis. *J. Climate*, **25**, 1587–1596, https://doi.org/10.1175/JCLI-D-11-00145.1.

Madonna, E., G. Hes, C. Li, C. Michel, and P. Y. F. Siew, 2020: Control of Barents Sea wintertime cyclone variability by large-scale atmospheric flow. *Geophys. Res. Lett.*, **47**, e2020GL090322, https://doi.org/10.1029/2020GL090322.

——, D. S. Battisti, C. Li, and R. H. White, 2021: Reconstructing winter climate anomalies in the Euro-Atlantic sector using circulation patterns. *Wea. Climate Dyn.*, **2**, 777–794, https://doi.org/10.5194/wcd-2-777-2021.

Manney, G. L., and M. I. Hegglin, 2018: Seasonal and regional variations of long-term changes in upper-tropospheric jets from reanalyses. *J. Climate*, **31**, 423–448, https://doi.org/10.1175/JCLI-D-17-0303.1.

——, ——, W. H. Daffer, M. J. Schwartz, M. L. Santee, and S. Pawson, 2014: Climatology of upper tropospheric–lower stratospheric (UTLS) jets and tropopauses in MERRA. *J. Climate*, **27**, 3248–3271, https://doi.org/10.1175/JCLI-D-13-00243.1.

Martius, O., 2014: A Lagrangian analysis of the Northern Hemisphere subtropical jet. *J. Atmos. Sci.*, **71**, 2354–2369, https://doi.org/10.1175/JAS-D-13-0329.1.

Pena-Ortiz, C., D. Gallego, P. Ribera, P. Ordonez, and M. D. C. Alvarez-Castro, 2013: Observed trends in the global jet stream characteristics during the second half of the 20th century. *J. Geophys. Res. Atmos.*, **118**, 2702–2713, https://doi.org/10.1002/jgrd.50305.

Schiemann, R., D. Lüthi, and C. Schär, 2009: Seasonality and interannual variability of the westerly jet in the Tibetan Plateau region. *J. Climate*, **22**, 2940–2957, https://doi.org/10.1175/2008JCLI2625.1.

Spensberger, C., 2023a: ERA5 jet axes 1979-2022 (dataset). Norstore, accessed 10 November 2023, https://doi.org/10.11582/2023.00120.

——, 2023b: ERA5 jet cross sections (dataset). Norstore, accessed 10 November 2023, https://doi.org/10.11582/2023.00121.

——, and T. Spengler, 2020: Feature-based jet variability in the upper troposphere. *J. Climate*, **33**, 6849–6871, https://doi.org/10.1175/JCLI-D-19-0715.1.

——, ——, and C. Li, 2017: Upper-tropospheric jet axis detection and application to the boreal winter 2013/14. *Mon. Wea. Rev.*, **145**, 2363–2374, https://doi.org/10.1175/MWR-D-16-0467.1.

Vallis, G. K., 2006: *Atmospheric and Oceanic Fluid Dynamics*. 1st ed. Cambridge University Press, 769 pp.

White, R. H., C. Hilgenbrink, and A. Sheshadri, 2019: The importance of Greenland in setting the northern preferred position of the North Atlantic eddy-driven jet. *Geophys. Res. Lett.*, **46**, 14 126–14 134, https://doi.org/10.1029/2019GL084780.

Winters, A. C., D. Keyser, and L. F. Bosart, 2020a: Composite vertical-motion patterns near North American polar–subtropical jet superposition events. *Mon. Wea. Rev.*, **148**, 4565–4585, https://doi.org/10.1175/MWR-D-20-0140.1.

——, ——, ——, and J. E. Martin, 2020b: Composite synoptic-scale environments conducive to North American polar–subtropical jet superposition events. *Mon. Wea. Rev.*, **148**, 1987–2008, https://doi.org/10.1175/MWR-D-19-0353.1.

Woollings, T., A. Hannachi, and B. Hoskins, 2010: Variability of the North Atlantic eddy-driven jet stream. *Quart. J. Roy. Meteor. Soc.*, **136**, 856–868, https://doi.org/10.1002/qj.625.

Yamada, R., and O. Pauluis, 2015: Annular mode variability of the atmospheric meridional energy transport and circulation. *J. Atmos. Sci.*, **72**, 2070–2089, https://doi.org/10.1175/JAS-D-14-0219.1.

——, and ——, 2016: Momentum balance and Eliassen–Palm flux on moist isentropic surfaces. *J. Atmos. Sci.*, **73**, 1293–1314, https://doi.org/10.1175/JAS-D-15-0229.1.